Partitioning and Voltage Control of High-Permeability Photovoltaic Distribution Network Considering Flexible Load-Side Resources

Wuyi Zhou[1,*], Chuang Liu[1], Dongbo Guo[2], Ruifeng Li[1] and Yu Wu[1]

[1]*School of Electrical Engineering, Northeast Electric Power University, Jilin, Jilin, 132012, China*
[2]*Tsinghua University, Beijing, 100084, China*
E-mail: 2202300196@neepu.edu.cn
[*]*Corresponding Author*

Received 04 March 2026; Accepted 28 April 2026

Abstract

The increasing penetration of distributed photovoltaics (*PV*) into distribution grids has led to a pronounced voltage over-limit issue, posing significant challenges to grid stability and power quality. Given this context, to address voltage management, a partition-based control methodology is proposed that leverages flexibility from load-side resources. Firstly, the double-layer probability fitting is carried out for photovoltaic uncertainty. Secondly, the risk indicators are innovatively proposed, and a dynamic zoning system including risk indicators is constructed. The centralized-distributed hybrid voltage control architecture suitable for dynamic partition is constructed again. Finally, the proposed model and its performance are assessed through

Distributed Generation & Alternative Energy Journal, Vol. 41_4, 1055–1078.
doi: 10.13052/dgaej2156-3306.4148

simulations on a modified IEEE 33-bus distribution network. The proposed algorithm effectively mitigates voltage deviations and enables flexible, efficient partition-based voltage control in modernized distribution systems.

Keywords: High permeability photovoltaic, distribution network, flexible resources, dynamic partition.

1 Introduction

As distribution networks are rapidly transitioning to become more active and interactive, the large-scale access of flexible resources such as distributed photovoltaic, energy storage and flexible load on the load side has made profound changes in the structure and operation characteristics of the distribution network [1–4]. In this context, the continuous increase of photovoltaic penetration leads to the increasingly prominent intermittency and volatility of its output. Consequently, power flows in the distribution network become bidirectional and stochastic, leading to more severe voltage fluctuations and frequent violations of limits [5–8].

The centralized voltage control method is often based on global information to optimize the calculation and uniformly allocate controllable resources. However, there are some defects including long control cycles, substantial data requirements, heavy communication loads, and considerable costs. The large-scale integration of decentralized, high-penetration resources significantly increases both the control variables and solution complexity for future distribution networks, thereby making the limitations of the centralized control mode increasingly apparent [9–18]. In order to cope with the above challenges, the partitioned voltage control architecture shows significant advantages through the organic combination of intra-regional self-regulation and inter-regional coordination. In reference [19], a holistic electrical distance metric, regional coupling intensity, and regional reactive power equilibrium indicator have been formulated for the distribution network, but regulating devices are only photovoltaics and SVCs. Although a dynamic partitioning method is developed in [20] for real-time scheduling, it focuses merely on the dynamic reactive power characteristics of resources like *PV* and storage, without accounting for other flexible assets. In reference [21], the regional autonomy index is constructed based on uncertainty when partitioning, but there is no response to the failure of regional autonomy in voltage control. Reference [22] combines partition with multi-time scale control, considers uncertainty in partition, and calls a variety of resources, but still does not show uncertainty as an indicator.

This work partitions the distribution network by leveraging the diverse response characteristics of flexible load-side resources. The proposed partitioning method begins by applying a two-layer probabilistic model to construct the probability distribution of *PV* generation forecast errors, and then the probability density function is fitted by normal distribution, t distribution, Kernel Density Estimation (KDE) and Diffusion Kernel Density Estimation (KDED) respectively. The distribution with the best fitting performance is selected from the perspective of data to overcome the limitation of single distribution hypothesis. Secondly, the uncertainty is innovatively expressed as a risk index, and a comprehensive evaluation system integrating regional structural, functional and risk indicators is constructed with the genetic algorithm performing the optimization, so as to enhance the adaptability of the partition scheme to the dynamic changes of the system operating conditions. Ultimately, a centralized-distributed hybrid control strategy that harnesses dynamic partitioning is proposed to facilitate more flexible and coordinated voltage regulation.

2 Dynamic Partition of Flexible Resources on the Load Side of High Permeability Photovoltaic Distribution Network

The purpose of dynamic partitioning is to make full use of various control resources better regulate the voltage.

2.1 Load-Side Flexible Resource Modeling

(1) Distributed photovoltaic

$$\begin{cases} 0 \le P_{j,t}^{PV} \le P_{j,t}^{PV,\max} \\ Q_{j,t}^{PV} = P_{j,t}^{PV} \times \tan\theta_{PV}, \quad \forall j \in N^{PV} \\ \Delta P_{j,t}^{PV,\max} = \alpha P_{j,t}^{PV} \end{cases} \tag{1}$$

In the formula: $P_{j,t}^{PV}$ and $Q_{j,t}^{PV}$ are the active power and the reactive power emitted by photovoltaic *j* at time *t*, respectively; $P_{j,t}^{PV,max}$ is the maximum active power of photovoltaic *j* at time *t*; $tan_{\theta PV}$ is the photovoltaic power factor; N^{PV} is the number of *PV*s in the network; $\Delta P_{j,t}^{PV,max}$ is the maximum reduction power of photovoltaic *j* at time *t*; for the proportion of abandoned light, this paper takes 20%.

(2) Distributed energy storage

$$\begin{cases} S_{SOC\min} \leq S_{SOC}(t) \leq S_{SOC\max} \\ -v_{ESS}^{down} \leq S_{SOC}(t+1) - S_{SOC}(t) \leq v_{ESS}^{up} \\ S_{SOC}(0) = S_{SOC}(\text{end}) \end{cases} \tag{2}$$

$S_{SOC}(t)$ denotes the state of charge of *ESS* at time *t*. The parameters S_{SOCmax} and S_{SOCmin} are defined as the upper and lower bounds for the energy storage system's charging power. The v_{ESS}^{down} and v_{ESS}^{up} represent the maximum discharge power and charging power per hour; $S_{SOC}(0)$ and $S_{SOC}(end)$ denote the state of charge at the initial and end of the scheduling, respectively.

(3) Flexible load

$$\begin{cases} 0 \leq P_{j,t}^{tr,in} \leq P_{j,t}^{tr,in,\max} L_{j,t}^{tr} \\ \sum_{t=1}^{T} P_{j,t}^{tr,in} = \sum_{t=1}^{T} P_{j,t}^{tr,out} \\ 0 \leq P_{j,t}^{tr,out} \leq P_{j,t}^{tr,out,\max}(1 - L_{j,t}^{tr}) \end{cases} \tag{3}$$

In the formula: $P_{j,t}^{tr,in,max}, P_{j,t}^{tr,out,max}$ are the maximum power that the transferable load can be transferred into and the maximum power that can be transferred out; $L_{j,t}^{tr}$ is the state variable of transferable load *j*.

$$P_{j,t}^{CU,\min} \leq P_{j,t}^{CU} \leq P_{j,t}^{CU,\max} \tag{4}$$

In the formula: $P_{j,t}^{CU,max}, P_{j,t}^{CU,min}$ are defined as the upper and lower bounds of the reducible load *j* at time *t*.

2.2 Dynamic Regional Division Index

In order to optimize the partition structure, this section innovatively proposes risk indicators and constructs a comprehensive index system that integrates structure, electrical characteristics and risks.

(1) Modularity indicator

The modularity function is used to measure the community structure strength of the partition structure, which can automatically generate the optimal number of partitions without presetting. It is defined as follows:

$$\rho = \frac{1}{2m} \sum_{i} \sum_{j} \left[A_{ij} - \frac{k_i k_j}{2m} \right] \delta(i, j) \tag{5}$$

In the formula, A_{ij} is the weight of the edge connecting the node *i* and the node. When the node *i* is directly connected to the node, $A_{ij} = 1$, and when it is not connected, $A_{ij} = 0$. If the node *i* and the node *j* are in the same partition, the function $\delta(i, j) = 1$, otherwise $\delta(i, j) = 0$.

(2) Regional voltage regulation capability indicator

Voltage limit violations emerge as the primary concern following the integration of a high proportion of distributed photovoltaics into the distribution network. A regional voltage regulation capability index is defined. It serves to characterize how the adjustable active and reactive power from flexible resources within a region can mitigate the maximum voltage deviation.

$$\varphi_{i,t}^{V} = \begin{cases} 1, & \Delta V_{i,t} \leq \Delta V_{i,t}^{max} \\ \dfrac{\Delta V_{i,t}^{max}}{\Delta V_{i,t}}, & \Delta V_{i,t} > \Delta V_{i,t}^{max} \end{cases} \tag{6}$$

$$\Delta V_{i,t}^{max} = \sum_{j \in N} (S_{VP,ij} \cdot \Delta P_{j,t}^{max} + S_{VQ,ij} \cdot \Delta Q_{j,t}^{max}) \tag{7}$$

$$\Delta P_{j,t}^{max} = \Delta P_{pv,j,t} + P_{ess,j,t} + \Delta P_{load,j,t} \tag{8}$$

$$\Delta Q_{j,t}^{max} = \Delta Q_{pv,j,t} + Q_{ess,j,t} + \Delta Q_{load,j,t} \tag{9}$$

The objective for each region is to mitigate voltage limit violations and minimize network losses from cross-regional power flow. This is achieved by fully utilizing internal resources via coordinated active and reactive power control. The overall voltage regulation capability of the system is calculated by the average value of each regional capability index, as shown in formula (10).

$$\varphi_{V} = \frac{1}{A_n} \sum_{i \in \Omega_n} \varphi_{i,t}^{V} \tag{10}$$

In formula (10): $\varphi_{i,t}^{V}$ and φ_{v} respectively represent the voltage regulation capability index of node I and region n; The variable Ω_n indicates the number of nodes contained in region n; $\Delta V_{i,t}^{max}$ represents the maximum voltage regulation of node *i* when considering the active and reactive power margin in the region; $S_{ij}^{VP,}$ and $S_{ij}^{VQ,}$ represent the active/reactive voltage sensitivity matrix, respectively. N represents the number of regions divided.

(3) Risk measurement indicator

The current partition optimization focuses more on deterministic evaluation, but the high uncertainty of photovoltaic power generation and power load brings additional operational risks to the system. Therefore, a risk measurement index based on Conditional Value-at-risk (*CVaR*) is introduced to quantify the risk exposure level of extreme voltage deviation under the partition results.

The calculation of the risk index is preceded by a probabilistic representation of both *PV* and load prediction errors. Then a two-layer probability model of photovoltaic error and a load forecasting error model are established to provide a basis for the calculation of subsequent risk indicators.

Accurately quantifying the uncertainty of photovoltaic output is a prerequisite for implementing efficient voltage control in high-permeability photovoltaic distribution networks. Traditional research methods often assume that the prediction error obeys a single normal distribution. However, the actual operation data show that the probability distribution characteristics of the prediction error show significant time-varying and numerical correlation, that is, its distribution pattern changes dynamically with the difference of prediction time and prediction output level. This study develops a two-layer probabilistic modeling method that overcomes the limitations of traditional approaches and provides a more accurate description of such complex uncertainty characteristics.

The first layer of the modeling framework aims to deal with the time correlation of prediction errors. The first step involves collecting the historical data of the total measured and total predicted power from the distributed photovoltaic systems, and all the data are arranged as the prediction error data set D_{PV} shown in formula (11) according to the prediction time point.

$$D_{\mathrm{pv}} = \begin{bmatrix} P_{\mathrm{pv\_err\_1}}^{\mathrm{t1}} & P_{\mathrm{pv\_err\_1}}^{\mathrm{t2}} & \cdots & P_{\mathrm{pv\_err\_1}}^{\mathrm{ti}} & \cdots & P_{\mathrm{pv\_err\_1}}^{\mathrm{tn}} \\ P_{\mathrm{pv\_err\_2}}^{\mathrm{t1}} & P_{\mathrm{pv\_err\_2}}^{\mathrm{t2}} & \cdots & P_{\mathrm{pv\_err\_1}}^{\mathrm{ti}} & \cdots & P_{\mathrm{pv\_err\_1}}^{\mathrm{tn}} \\ \cdots & \cdots & \cdots & \cdots & \cdots & \cdots \\ P_{\mathrm{pv\_err\_k}}^{\mathrm{t1}} & P_{\mathrm{pv\_err\_k}}^{\mathrm{t2}} & \cdots & P_{\mathrm{pv\_err\_k}}^{\mathrm{ti}} & \cdots & P_{\mathrm{pv\_err\_k}}^{\mathrm{tn}} \\ \cdots & \cdots & \cdots & \cdots & \cdots & \cdots \\ P_{\mathrm{pv\_err\_m}}^{\mathrm{t1}} & P_{\mathrm{pv\_err\_m}}^{\mathrm{t2}} & \cdots & P_{\mathrm{pv\_err\_m}}^{\mathrm{ti}} & \cdots & P_{\mathrm{pv\_err\_m}}^{\mathrm{tn}} \end{bmatrix} \tag{11}$$

$$P_{\mathrm{pv\_err\_k}}^{\mathrm{ti}} = P_{\mathrm{pv\_pre\_k}}^{\mathrm{ti}} - P_{\mathrm{pv\_act\_k}}^{\mathrm{ti}} \tag{12}$$

Where $P_{tiPV\_err\_k}$ denotes the prediction error at the i prediction moment on day k. Firstly, the historical data are grouped according to the prediction time, and then the *Wasserstein* distance is used as a measure of the difference between the prediction error distribution in different periods. Based on the distance matrix, K-means clustering aggregates the time points of a day into several categories sharing similar distribution characteristics. The clustering number *n* is objectively determined by the contour coefficient method, and the boundary time points between the categories obtained will be used as the trigger conditions for the subsequent dynamic partitioning strategy.

For each category obtained by time clustering, the numerical correlation of prediction errors is further considered. In view of the fact that the error distribution pattern is often closely related to the size of the predicted output value, this study uses the three-digit division method to divide the photovoltaic output prediction value sequence into three continuous intervals ($Q_1 = 33.3\%$, $33.3\% < Q_2 = 66.6\%$, $Q_3 > 66.6\%$) with equal probability in each time category. Finally, the data of the whole day is divided into 3n data sets with homogeneity.

For each group, four probability models, KDED, KDE, normal distribution and t distribution, are applied to approximate the prediction error's probability density function. According to the goodness of fit of different models on each group of data, the optimal fitting scheme is selected.

The load forecasting error obeys the normal distribution, and for the load forecasting error, its probability density function is:

$$\begin{cases} f(P_{\text{load}}) = \dfrac{1}{\sqrt{2\pi}\sigma_{\text{P}}} \exp\left(-\dfrac{(P_{\text{load}} - \mu_{\text{P}})^2}{2\sigma_{\text{P}}^2}\right) \\ f(Q_{\text{load}}) = \dfrac{1}{\sqrt{2\pi}\sigma_{\text{Q}}} \exp\left(-\dfrac{(Q_{\text{load}} - \mu_{\text{Q}})^2}{2\sigma_{\text{Q}}^2}\right) \end{cases} \tag{13}$$

In the formula, the active and reactive loads are denoted by P_{load} and Q_{load}, respectively. Their mean values and standard deviations are represented by μ_P, σ_P, and μ_Q, σ_Q.

After the source-load uncertainty is processed, the risk index is calculated.

Define the node voltage deviation loss function:

$$L_{j,i}^{k} = max\left(0, \frac{|V_{j,i} - V_{nom}|}{V_{nom}} - \varepsilon_{allow}\right) \tag{14}$$

In the formula, $V_{j,i}$ is the voltage amplitude of node *j* under scenario *i*, V_{nom} is the nominal voltage of the system, and ε_{allow} is the allowable voltage deviation limit, which is taken as $\pm$ 0.05.

Then the partition weighted total loss is calculated

$$L_i^k = \sum w_j \cdot L_{j,i}^k \tag{15}$$

$$w_j = \frac{S_{load,j}}{\sum_{m \in k} S_{load,m}} \tag{16}$$

$$S_{load,j} = max\sqrt{P_{load,j}(t)^2 + Q_{load,j}(t)^2} \tag{17}$$

The node weight w_j is based on load capacity allocation, and Sload, *j* represents the load capacity of node *j*. Finally, the conditional risk value of partition *k* is the conditional expectation that the loss exceeds the risk value at the confidence level, and its normalized risk index is:

$$CVaR_\alpha^k = \frac{1}{N - \lfloor \alpha \cdot N \rfloor + 1} \sum_{i=\lceil \alpha \cdot N \rceil}^{N} L_{(i)}^k \tag{18}$$

$$\varphi_R = \frac{CVaR_\alpha^k}{\sum_{j \in k} S_{load,j}} \tag{19}$$

In the formula, *CVaRka* is the conditional risk value considering the interval error, and φ_R is the normalized risk index.

Integrating the above three indicators, a comprehensive zoning evaluation index is constructed:

$$\rho_{\mathrm{com}} = \omega_1 \rho + \omega_2 \varphi_V + \omega_3 (1 - \varphi_R) \tag{20}$$

In the formula: $\omega_1, \omega_2, \omega_3$ are the weight coefficients of the three indicators, $\omega_1 + \omega_2 + \omega_3 = 1$.

To optimize the comprehensive index, the Particle Swarm Optimization (PSO) algorithm is adopted [18].

Based on the dynamic partition scheme obtained above, the following section designs a centralized-distributed hybrid voltage control architecture. The partition results, including region boundaries, resource assignments, and risk assessments, are directly transmitted to the virtual controllers as structural inputs for distributed optimization. This linkage ensures that the control strategy adapts in real time to the evolving partition topology.

3 Centralized-Distributed Hybrid Voltage Control Strategy Based on Dynamic Partition

Receiving the partition topology generated by the dynamic partitioning framework in Section 2, the centralized-distributed hybrid control architecture operates as follows.

A centralized-distributed hybrid voltage control architecture is designed in this section. The core of this architecture is that the central controller is responsible for system-level coordination and boundary consistency constraint management, while the virtual controllers of each partition are based on the augmented Lagrangian alternating direction method to solve the optimization problems in their jurisdictions in parallel. This design effectively peels off the global coupling and realizes distributed computing, which significantly improves the computational efficiency while ensuring the global optimization effect.

3.1 Centralized-Distributed Hybrid Voltage Control Architecture Design

The control architecture proposed in this paper can be decomposed into three core links:

Step 1: Based on the predicted data, the optimal partition scheme of the current period is generated. The central controller sends the partition scheme to each virtual controller in the network.

Step 2: After receiving the partition scheme, each virtual controller solves the optimization problem of the region in parallel based on the Simplified Alternating Direction Method of Multipliers (SADMM) algorithm whose objective function is minimizing network loss, voltage deviation and photovoltaic reduction.

Step 3: Each virtual controller obtains a distributed optimization result and performs voltage verification. When the optimization is successful, the control command is issued; when the optimization fails, the central controller performs global optimization with the minimum voltage deviation to obtain the control

3.2 Optimal Control Model

Based on the partition results, the virtual controllers of each partition need to coordinate and optimize the flexible resources in the partition under the premise of satisfying all the safe operation constraints, so as to achieve multiple goals such as system voltage level improvement and power loss reduction.

(1) Optimizing the objective function

Minimum the network loss:

$$f_1 = \min \mathrm{P}_{loss} = \sum_{\mathrm{t}=1}^{T} P_{loss,t} \tag{21}$$

In the formula: $P_{loss,t}$ is the active power loss of the grid at time *t*.

Minimum the voltage deviation:

$$f_2 = \min \sum_{t=1}^{T} |U_{i,t}^2 - U_{\mathrm{N}}^2| \tag{22}$$

In the formula: $U_{i,t}$ is the voltage amplitude of node *i* in *t* period; U_N is the rated voltage of node.

Minimum the photovoltaic reduction:

$$f_3 = \min \sum_{t=1}^{T} \sum_{i \in N_{\mathrm{PV}}} (P_{i,t}^{PV,\max} - P_{i,t}^{PV}) \tag{23}$$

In the formula: $P_{i,t}^{PV,max}$ and $P_{i,t}^{PV}$ are the maximum active power output and the actual active power output of $PV\ i$ at time *t*, respectively; N_{PV} is the set of photovoltaic access nodes in the system.

$$f = \min(\eta_1\gamma_1 f_1 + \eta_2\gamma_2 f_2 + \eta_3\gamma_3 f_3) \tag{24}$$

In the formula, $\eta_1 - \eta_3$ are the weight coefficients and $\eta_1 + \eta_2 + \eta_3 = 1$; $\gamma_1 - \gamma_3$ are the correction coefficients greater than 0.

(2) Constraint conditions

In this paper, the general DistFlow power flow model is used, and The formulation of the power flow constraints is given in Equation (25):

$$\begin{cases} P_{\mathrm{g}i} - P_{\mathrm{d}i} - U_i \sum_{j \in i} U_j (G_{ij} \cos\theta_{ij} + B_{ij} \sin\theta_{ij}) = 0 \\ Q_{\mathrm{g}i} - Q_{\mathrm{d}i} - U_i \sum_{j \in i} U_j (G_{ij} \sin\theta_{ij} - B_{ij} \cos\theta_{ij}) = 0 \end{cases} \tag{25}$$

In the formula: At node i, $P_{\mathrm{g}i}$ and $Q_{\mathrm{g}i}$ are the active and reactive power outputs, $P_{\mathrm{d}i}$ and Q_{di} the corresponding loads, and U_i the voltage magnitude. For branch $i-j$, G_{ij}, B_{ij} and θ_{ij} denote the conductance, susceptance, and phase angle difference, respectively.

The voltage constraint is shown in Equation (26):

$$U_{i,t}^{\min} \leq U_{i,t} \leq U_{i,t}^{\max} \tag{26}$$

In the formula: $U_{i,t}$ is the voltage at time t of i node, $U_{i,t}^{min}$ and $U_{i,t}^{max}$ are the upper and lower limits of node voltage respectively.

The constraint conditions of flexible resources on the load side are shown in Formula (1)–(4).

3.3 Model Solving Method Based on SADMM

In order to efficiently solve the above optimization model, it is decoupled into multiple sub-problems according to the dynamic partition results, and the SADMM algorithm is used for distributed solution.

In order to construct a SADMM algorithm suitable for distribution network partition, it is necessary to first remove the coupling relationship between different partitions. The partition decoupling procedure is presented schematically in Figure 1, and the three adjacent regions are taken as examples to illustrate that the ab region is related to each other through the connection line between nodes *i* and *j*. The specific operation is to cut off

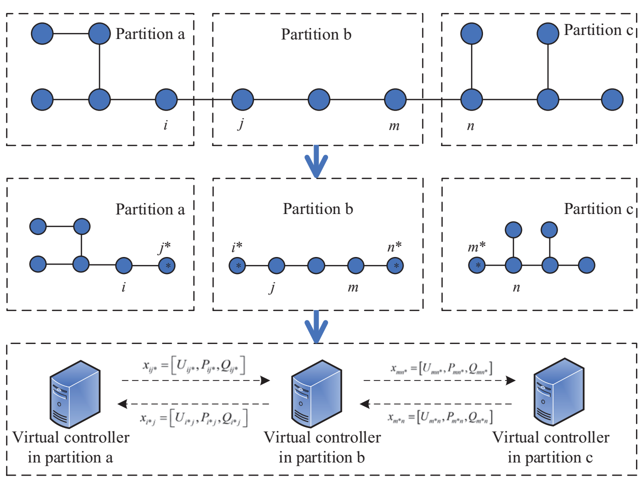

Figure 1 Distribution network partition decoupling flow chart.

the connection line between nodes i and j, and replace the original i and j nodes with virtual nodes i* and j* respectively, thus forming virtual boundary connection lines i*j and ij*. Using the same method, the virtual boundary connection lines m*n and mn* between partitions b and c can be obtained. The introduction of virtual nodes will not affect the running state of the original nodes, thus completing the decoupling processing of the distribution network.

In the solution process, each partition performs independent parallel operations, and only the data exchange of consistency variables with adjacent partitions is required. The consistency variables for the virtual boundary link are defined as the line's voltage magnitude, active power, and reactive power. The consistency variables of the two adjacent partitions are the active power, reactive power and voltage values on the virtual boundary connection line. Each partition only needs to transmit a small amount of boundary information, which effectively reduces the communication load in the data transmission process and reduces the operation time.

Using the 'decomposition-coordination' principle, the optimization problem of the entire distribution network is decomposed into sub-problems with boundary coupling constraints in each sub-region. Based on the optimization model established, the control model based on the SADMM optimization method is constructed as follows:

$$\begin{cases} \min \sum_{a}^{N} f_a(\boldsymbol{x}_a) \\ \text{s.t.} \quad \boldsymbol{h}_a(\boldsymbol{x}_a) = 0, \quad K = 1, 2, \ldots, N \\ \qquad \boldsymbol{g}_a(\boldsymbol{x}_a) \geq 0, \quad K = 1, 2, \ldots, N \end{cases} \tag{27}$$

In (27): $f_a(\boldsymbol{x}_a)$ is the objective function of the subproblem of partition a, which is a convex function; $\boldsymbol{h}_a(\boldsymbol{x}_a)$ is the equality constraint of the partition a subproblem, which is a linear function; $\boldsymbol{g}_a(\boldsymbol{x}_a)$ is an inequality constraint for the subproblem of partition a.

The Lagrangian transformation of pair (28) yields:

$$\varsigma_K = f_a(\boldsymbol{x}_a) + (\boldsymbol{\lambda}_{a,b,ij})^{\mathrm{T}}(\boldsymbol{x}_{a,b,ij} - \boldsymbol{x}_{b,a,ij}) + 0.5\rho\|\boldsymbol{x}_{a,b,ij} - \boldsymbol{x}_{b,a,ij}\|_2^2 \tag{28}$$

In the formula: $\rho > 0$ is the penalty coefficient; $\boldsymbol{\lambda}_{a,b,ij}$ are dual variables; stretching $\boldsymbol{\lambda}_{a,b,ij}$ to $(\rho/1)\boldsymbol{\lambda}_{a,b,ij}$, and omitting the constant term, then it can be transformed into

$$s_K = f_a(\boldsymbol{x}_a) + 0.5\rho\|\boldsymbol{x}_{a,b,ij} - \boldsymbol{x}_{b,a,ij} + \boldsymbol{\mu}\|_2^2 \tag{29}$$

In summary, the SADMM iterative solution process is:

$$\begin{aligned} \boldsymbol{x}_a^{k+1} &= \arg\min[f_a(\boldsymbol{x}_a) + 0.5\rho \parallel \boldsymbol{x}_{a,b,ij} - \boldsymbol{x}_{b,a,ij}^k + \boldsymbol{\mu}^k \parallel_2^2] \\ \boldsymbol{x}_b^{k+1} &= \arg\min[f_b(\boldsymbol{x}_b) + 0.5\rho \parallel \boldsymbol{x}_{a,b,ij}^{k+1} - \boldsymbol{x}_{b,a,ij} + \boldsymbol{\mu}^k \parallel_2^2] \\ \boldsymbol{\mu}^{k+1} &= \boldsymbol{\mu}^k + (\boldsymbol{x}_{a,b,ij}^{k+1} - \boldsymbol{x}_{b,a,ij}^k) \end{aligned} \tag{30}$$

In order to speed up the convergence rate, the average value of the sum of the previous calculation results of this partition and adjacent partitions is selected as the boundary condition of the next iteration. Therefore, in the kth iteration, the updating rules of boundary conditions and dual variables are as follows:

$$\hat{\boldsymbol{x}}_{a,b,ij}^{k+1} = \hat{\boldsymbol{x}}_{b,a,ij}^{k+1} = \frac{\boldsymbol{x}_{a,b,ij}^k + \boldsymbol{x}_{b,a,ij}^k}{2} \tag{31}$$

$$\begin{cases} \boldsymbol{\mu}_a^{k+1} = \boldsymbol{\mu}_a^k + (\boldsymbol{x}_a^{k+1} - \hat{\boldsymbol{x}}_b^{k+1}) \\ \boldsymbol{\mu}_b^{k+1} = \boldsymbol{\mu}_b^k + (\boldsymbol{x}_b^{k+1} - \hat{\boldsymbol{x}}_a^{k+1}) \end{cases} \tag{32}$$

Taking partition *a* as an example, the original residual and dual residual of the SADMM algorithm in this paper are defined as r_a^k, and s_a^k, respectively. The convergence criterion is defined as ε. In this paper, r_a^k, and s_a^k are less than as the convergence criterion of the algorithm. When the following equation is satisfied, it is considered that the iterative process of the algorithm in this paper ends:

$$r_a^k = \boldsymbol{x}_a^k - \hat{\boldsymbol{x}}_{a\infty}^k \leq \varepsilon \tag{33}$$

$$s_a^k = \boldsymbol{\mu}_{a,ij}^k - \boldsymbol{\mu}_{a,ij\infty}^{k-1} \leq \varepsilon \tag{34}$$

4 Simulation

The modified IEEE-33 is used as the test system for analysis, and the node situation is shown in Figure 2.

The simulation is conducted over a 24-hour day-ahead scheduling horizon with a time step resolution of 0.25 h. To quantify the risk associated with photovoltaic and load uncertainties, 2,000 Monte Carlo scenarios are generated, and the CVaR confidence level α is set to 0.95. For the SADMM-based distributed optimization, the penalty parameter ρ is set to 0.05 and the convergence tolerance ε is set to 1×10^{-4}. The PSO algorithm employed in the partition optimization phase uses a population size of 50 and a maximum

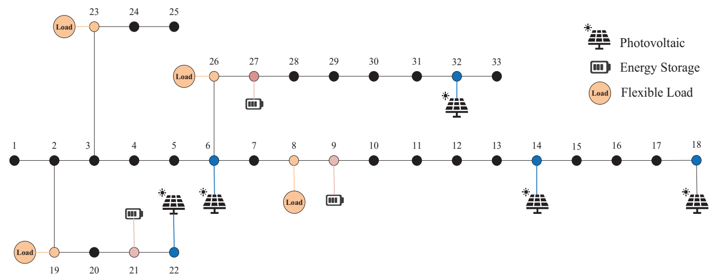

Figure 2 Improved IEEE 33-node topology diagram.

iteration count of 200. The partition weight coefficients for the comprehensive evaluation index are set as $\omega_1 = 0.3$, $\omega_2 = 0.4$, and $\omega_3 = 0.3$, while the control objective weight coefficients are $\eta_1 = 0.3$, $\eta_2 = 0.4$, and $\eta_3 = 0.3$. The node voltage is constrained within 0.95–1.05 p.u., and the maximum PV curtailment is limited to 20% of the maximum output. All simulations are performed on MATLAB 2022b with Gurobi 9.0.0 as the optimization solver.

4.1 Photovoltaic Uncertainty Processing Results and Verification

Based on the photovoltaic two-layer probability modeling method, Belgian photovoltaic data spanning June 1 to September 1, 2024, were selected for model training and validation. Since the photovoltaic output at night is zero, only non-zero output is processed.

Based on the method proposed above, the clustering results divide the day into five characteristic periods: 00:00–05:30 h, 05:30–09:15 h, 09:15–15:45 h, 15:45–20:30 h, 20:30–24:00 h. Among them, the photovoltaic output in the first and last time periods is 0.

In the non-zero time clustering category of photovoltaic output, the three quantiles are further grouped according to the predicted photovoltaic output value, and a total of 9 data groups are obtained. Figure 3 shows the probability density function fitting results of some of the groups. The analysis shows that the distribution of photovoltaic prediction error shows significant diversity. For approximately symmetrical unimodal distribution, normal distribution and t distribution can achieve good fitting; for complex distributions with multi-peak, skewed or heavy-tailed characteristics, KDE and KDED show more excellent adaptability by virtue of their flexibility without preset distribution forms.

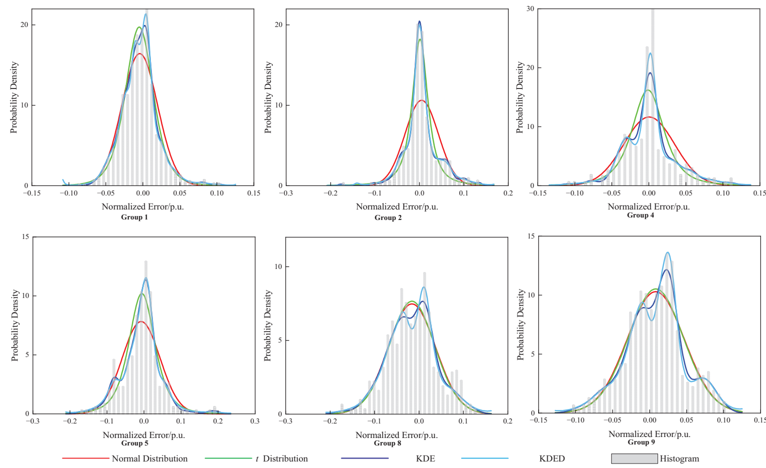

Figure 3 Photovoltaic prediction error probability distribution fitting.

Independent validation was performed using June-September 2025 data, and the results are shown below.

At the 90% confidence level, the coverage verification results based on the out-of-sample real operation data from the independent validation set are shown in the figure. It can be observed that the coverage obtained by the KDED method is the highest in the same group, generally higher than the nominal 90% confidence level, and it can be seen from Figure 4(b) that its interval width is also the largest in the same group. This shows that KDED can flexibly adjust the kernel bandwidth according to the distribution characteristics of the error data, and has a strong ability to capture extreme values by increasing bandwidth to improve coverage, which is especially suitable for the non-normal, heavy-tailed distribution of photovoltaic prediction errors in actual operation. The coverage of the KDE method is also mostly maintained at more than 90%, with the second-best overall performance. The coverage of normal distribution and t distribution fluctuates around the 90% confidence level with small amplitude, showing stable fitting performance for approximately symmetric unimodal error distributions, and their fitted confidence interval width is also relatively small. Based on the above results, this paper selects the optimal fitting method for each data group respectively, and the final selection scheme is shown in Table 1.

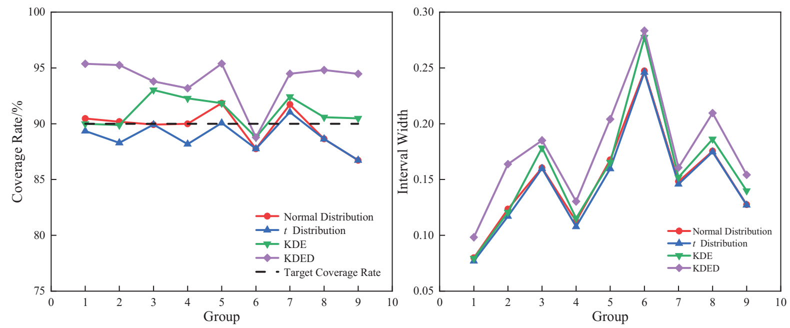

(a)coverage rate comparison (b)interval width comparison

Figure 4 Comparison of each fitting scheme for all the groups.

Table 1 Selection of fitting methods in each group

Group	Method	Group	Method	Group	Method
1	KDE	4	normal distribution	7	t distribution
2	normal distribution	5	t distribution	8	KDE
3	KDE	6	KDE	9	KDE

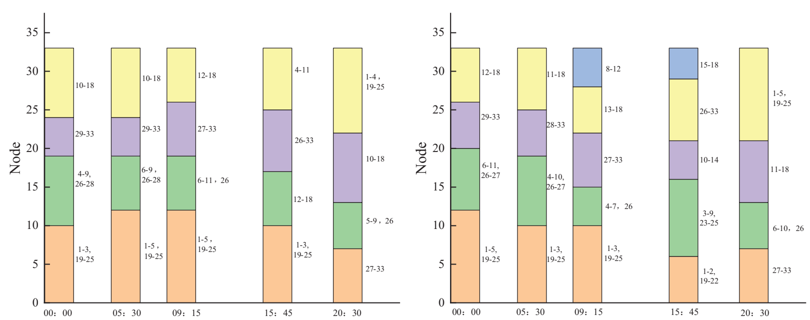

(a) scheme 1 (b) scheme 2

Figure 5 Partition results of two schemes.

4.2 Partition Results and Partition Rationality Analysis

In this paper, the zoning scheme obtained according to the index of Reference [21] is Scheme 1; the partition scheme obtained according to the index in this paper is scheme 2, as shown in Figure 5.

To evaluate the validity of the partition results, this paper utilizes the following constraint indicators, following [23].

(1) The connectivity index is defined as ensuring that nodes within a partition are fully interconnected, while being isolated from nodes in other partitions.
(2) The rationality criterion for the number of partitions requires that the optimal count in an n-node system not exceed $\sqrt{n}$.
(3) Reactive power source constraint: The partition must contain at least one reactive power source.

4.3 Effectiveness Analysis of Partitioned Voltage Control

This study compares the voltage stability performance of the two partitioning strategies. Four simulation cases are established to verify the effectiveness of the proposed model:

Case 1: No optimal control method is used for the distribution network.

Case 2: Optimal control of distribution networks solely through *PV* curtailment.

Case 3: A coordinated optimal control scheme is applied, utilizing both distributed *PV* curtailment and energy storage units within the distribution network.

Case 4: Integrated optimal control is applied to the distribution network via coordinated *PV* curtailment, energy storage dispatch, and flexible load adjustment.

Figure 6(a) is the node voltage optimization result at 13:30 in a scenario of scheme 1. It can be seen that in the AC distribution network without

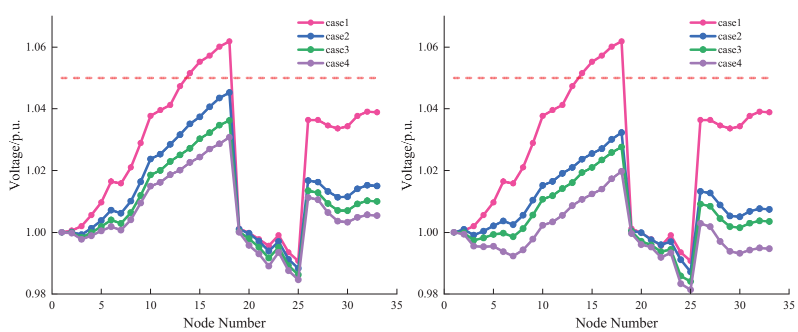

(a) The voltage control effect of scheme 1 (b) The voltage control effect of scheme 2

Figure 6 The voltage control effect of two schemes.

any optimal control method, due to the strong light intensity and the excess photovoltaic output at this time, thereby causing an overvoltage condition at several nodes within the system, while Case 2–4 can solve the problem of voltage violation. By comparing Case 3 with Case 2, it can be seen that the voltage level of some nodes in Case 3 has been significantly improved, while the node voltage in the corresponding Case 2 is still on the high side. Compared with Case 3, the voltage level of Case 4 has been further improved. Figure 6(b) is the node voltage optimization result at 13:30 in a scenario of scheme 2. Because scheme 2 considers the uncertainty of photovoltaic and load when partitioning, it can better match the spatial and temporal characteristics of the partition with the source and load, and each case is improved compared with scheme 2. As shown in Figure 6(b) for Case 4, the voltage is further reduced.

4.4 Computational Efficiency Analysis

The above simulation results have verified the superiority of the proposed partitioned voltage control strategy in suppressing voltage deviation and mitigating voltage over-limit issues. However, in practical engineering applications of active distribution networks, the computational efficiency and real-time performance of the algorithm are core indicators that determine its feasibility for online scheduling and closed-loop control. To substantiate the computational advantage of the proposed SADMM-based distributed optimization method in this paper, this subsection compares its convergence performance and computational efficiency against two mainstream benchmark methods: the standard ADMM algorithm and the centralized PSO-based optimization approach.

The computational performance metrics are summarized in Table 2.

The results show that the centralized PSO algorithm has the lowest computational efficiency, requiring 342 iterations to converge with a total time of 208.1 s. This is because the centralized method processes all system variables and constraints simultaneously, resulting in high optimization dimensionality and heavy solution complexity, which cannot meet the real-time demand of voltage control.

Table 2 Computational performance comparison of different algorithms

Method	Iterations	Total Time (s)
Centralized PSO	342	208.1
ADMM	38	43.7
SADMM	22	22.8

In contrast, the standard ADMM algorithm decomposes the global problem into parallel sub-problems of each partition based on the decoupling architecture, only exchanging a small amount of boundary information between adjacent partitions. It reduces iterations to 38 and total time to 43.7 s, a 79.0% reduction compared with centralized PSO, fully reflecting the efficiency advantage of the distributed architecture.

The proposed SADMM algorithm further optimizes the update rule of boundary consistency variables, significantly accelerating convergence. It only needs 22 iterations to converge, with a total time of 22.8 s. Compared with centralized PSO and standard ADMM, the calculation time is reduced by 89.0% and 47.8% respectively. The results prove that the proposed SADMM algorithm can greatly improve solution efficiency while ensuring global optimization, and has stronger engineering practical value for real-time voltage control of high-permeability photovoltaic distribution networks.

5 Conclusion

Aiming at the problem of voltage control in high-permeability photovoltaic distribution network, this paper proposes a load-side flexible resource collaborative control strategy that integrates dynamic partition and hybrid architecture. The main findings of this study are summarized below.

(1) A key innovation of this paper is the development of a two-layer probabilistic model for photovoltaic generation. By grouping modeling, it can better describe the uncertainty of photovoltaics and is more optimized than a single modeling method.
(2) Building on the consideration of *PV* and load uncertainties, this study develops a new risk index. At the same time, a comprehensive system integrating modularity, regional autonomy ability and the risk index is constructed. This example validates that the proposed strategy mitigates voltage issues more effectively than partitioning without risk consideration.
(3) A centralized-distributed hybrid control architecture is designed to address the dynamic partitioning challenge. The architecture relies on the distributed solution of the central coordination and virtual controller, which can better guarantee the global optimization performance.
(4) The proposed SADMM-based distributed solution algorithm optimizes the update rule of boundary consistency variables, and significantly improves the solution efficiency of the partitioned voltage control model.

While ensuring the voltage control effect, it greatly reduces the number of iterations and calculation time, has excellent real-time performance, and provides an efficient solution for online voltage management of high-permeability photovoltaic distribution networks.

Acknowledgements

This work is funded by the Jilin Provincial Natural Science Foundation for Distinguished Young Scholars (Grant No. 20230101354JC).

References

[1] Song G C, Wu Q W, Jiao W S, et al. "Distributed coordinated control for voltage regulation in active distribution networks based on robust model predictive control" [J]. International Journal of Electrical Power & Energy Systems, 2025, 166: 110529.
[2] Pan M Q, He X, Ai Q, et al. "Research status and prospect of distributed resource scheduling for new distribution systems" [J]. Power System Technology, 2024, 48(3): 933–948.
[3] Li J H, Zhao T, Sun D P, et al. "Multi-layer optimization method for siting and sizing of distributed energy storage in distribution networks based on cluster partition" [J]. Journal of Cleaner Production, 2025, 501: 145260.
[4] Chen D Q, Zhao G G, Wang X B, et al. "Research on the method of dynamic subarea division of road traffic networks based on floating car data" [J]. Physica A: Statistical Mechanics and its Applications, 2025, 675: 130832.
[5] Yang L Y, Ren X C, Cai Z P, et al. "Research on voltage control strategy of distribution network with high PV penetration" [J]. Power System Technology, 2024, 48(12): 5056–5070.
[6] Liu L, Zhu W, Yang X. "Research on Operation Mode of New Distribution System with Integrating Large Scales of Distributed Photovoltaic" [C]. // 2022 IEEE International Conference on Power Systems and Electrical Technology (PSET). Aalborg, Denmark: 2022: 347–352.
[7] Kang W F, Guan Y J, Wang H Y, et al. "Distributed control of virtual energy storage systems for voltage regulation in low voltage distribution networks subjects to varying time delays" [J]. Applied Energy, 2024, 376(Part B): 124295.

[8] Sundarajoo, S., and Soomro, D. M. "Artificial Neural Network-Based Voltage Stability Online Monitoring Approach for Distributed Generation Integrated" [J] Distribution System. Distributed Generation and Alternative Energy Journal, 2023, 38(6), 1839–1862.
[9] Fu, Y, Ma, Z., Wang, W., Yao, Z., Li, R., and Guo, D. "Voltage Coordinated Control Strategy for Distribution Networks Based on Multi-Time Scale Sequential Action Control" [J] Distributed Generation and Alternative Energy Journal, 2025, 40(3), 505–531.
[10] Li, H., Wang, C., Tian, H., Ren, Z., Zhao, E., and Xu, L. "A Multi-objective Optimization Planning Framework for Active Distribution System Via Reinforcement Learning". [J] Distributed Generation and Alternative Energy Journal, 2023, 38(6), 1741–1762.
[11] Kinga S, Megahed T F, Kanaya H, et al. "A new voltage sensitivity-based distributed feedback online optimization for voltage control in active distribution networks" [J]. Computers and Electrical Engineering, 2024, 119(Part A): 109574.
[12] Jiao W S, Wu Q W, Chen J, et al. "Analytical target cascading based real-time distributed voltage control for MV and LV active distribution networks" [J]. International Journal of Electrical Power & Energy Systems, 2024, 159: 110024.
[13] Babu K R, Khatod D K. "Analytical voltage sensitivity-based distributed Volt/Var control for mitigating voltage-violations in low-voltage distribution networks" [J]. Electric Power Systems Research, 2024, 228: 110015.
[14] Li G, Wang W, Pang D, et al. "A cloud-edge collaborative optimization control strategy for voltage in distribution networks with PV stations" [J]. International Journal of Electrical Power and Energy Systems, 2025, 167: 110632.
[15] Wu Z, Li Y Q, Zhang X, et al. "Distributed voltage control for multi-feeder distribution networks considering transmission network voltage fluctuation based on robust deep reinforcement learning" [J]. Applied Energy, 2025, 379: 124984.
[16] Li B L, Wu Q W, Cao Y J, et al. "Physically informed multi-agent deep reinforcement learning for distributed voltage control in distribution networks" [J]. International Journal of Electrical Power & Energy Systems, 2026, 174: 111451.
[17] Su J S, Zhang H C, Liu H, et al. "Lyapunov-based distributed secondary frequency and voltage control for distributed energy resources in islanded microgrids with expected dynamic performance improvement" [J]. Applied Energy, 2025, 377(Part C): 124539.

[18] Zhang B, Cao D, Hu W H, et al. "Physics-Informed Multi-Agent deep reinforcement learning enabled distributed voltage control for active distribution network using PV inverters" [J]. International Journal of Electrical Power & Energy Systems, 2024, 155(Part B): 109641.
[19] Wang H, Li W, Zhang Y, et al. "A multi-objective distribution network partitioned voltage active-reactive coordination control strategy based on Synchronous ADMM" [C]. // 2024 4th International Conference on Smart Grid and Energy Internet (SGEI). Shenyang, China: 2024: 289–294.
[20] Li W R, Zuo X R, Ju L R, et al. "Research on Partitioning Real-Time Reactive Power Optimization Method for Distribution Network with Renewable Energy" [C]. // 2022 5th International Conference on Power and Energy Applications (ICPEA). Guangzhou, China: 2022: 360–364.
[21] Wang J J, Yao L Z, Liu K X, et al. "Method for dynamic region division of distribution network for regional autonomy" [J]. Power System Technology, 2024, 48(11): 4699–4709.
[22] Li P, Zhang H, Zhao S S, et al. "An optimal allocation method for power distribution network partitions based on improved spectral clustering algorithm" [J]. Engineering Applications of Artificial Intelligence, 2023, 123(Part C): 106497.
[23] Sun Y F. "The optimization strategy of intra-district autonomy based on stable partition under the scenario of high proportion of photovoltaic access to distribution network" [D]. Northeast Electric Power University, 2025.

Biographies

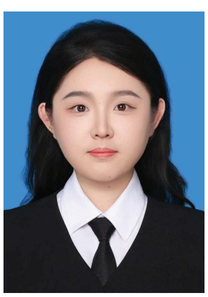

Wuyi Zhou, female, is currently a master's degree candidate in Electrical Engineering at Northeast Electric Power University. Her primary research focus lies in voltage control of distribution grids.

Chuang Liu, male, is currently a doctoral supervisor and professor in Electrical Engineering at Northeast Electric Power University. His primary research focus lies in flexible operation and control of distribution grids.

Dongbo Guo, male, is currently an in-service postdoctoral researcher at Tsinghua University. His research primarily focuses on direct AC/AC power conversion theory and its applications.

Ruifeng Li, male, is currently a doctoral candidate at Northeast Electric Power University. His research primarily focuses on direct AC/AC power conversion technology and its application in multimodal control of distribution grids.

Yu Wu, male, is currently a master's degree candidate in Electrical Engineering at Northeast Electric Power University. His primary research focus lies in transient voltage control.